Clinical Radiology 93 (2026) 107114

Contents lists available at ScienceDirect

Clinical Radiology

journal homepage: www.clinicalradiologyonline.net

Exploring the diagnostic value of dynamic contrast-enhanced and diffusion tensor imaging of intratumoural and peritumoural high-grade gliomas for distinguishing treatment response from tumour progression

Y. Diao [a,b,†], H. Liang [c,†], Y. Wang [d], L. Hang [a,b], L. Fang [a,b], H. Qu [a,b], H. Sun [a,b], W. Li [a,b], G. Jiang [a,b,*]

[a] *The Affiliated Guangdong Second Provincial General Hospital of Jinan University, School of Medicine, Jinan University, Guangzhou, 510632, China*
[b] *The Department of Medical Imaging, Guangzhou Key Laboratory of Molecular Functional Imaging and Artificial Intelligence for Major Brain Diseases, Guangdong Second Provincial General Hospital, Guangzhou 518037, China*
[c] *Department of Radiology, Shandong Cancer Hospital and Institute, Shandong First Medical University and Shandong Academy of Medical Sciences, Jinan, 250117, China*
[d] *Department of Radiology, Qingdao Hospital, University of Health and Rehabilitation Sciences(Qingdao Municipal Hospital), Qingdao, 266104, China*

ARTICLE INFORMATION

Article history:
Received 24 December 2024
Received in revised form
9 August 2025
Accepted 30 September 2025

AIM: Accurate differentiation true true progression (TP) and treatment response (TR) in high-grade gliomas (HGGs) remains challenging due to confounding alterations in tumour parenchymal areas. Evaluation of non-enhancing peritumoural regions (NEPTRs) plays a prominent role. This study aimed to assess diagnostic accuracy in distinguishing TP from TR by quantifying perfusion and diffusion differences in NEPTRs imaged with dynamic contrast-enhanced magnetic resonance imaging (DCE-MRI) and diffusion tensor imaging (DTI).

MATERIALS AND METHODS: Patients who had newly enhanced lesions or had developed enhanced lesions were retrospectively enrolled. All patients had undergone conventional imaging sequences, DTI, and DCE. Histopathological diagnosis or longitudinal clinical and imaging follow-up over 6 months was used to distinguish TP from TR. Volume transfer contrast (Ktrans), extravascular extracellular volume fraction (Ve), initial area under the time concentration curve (iAUC), fractional anisotropy (FA), and apparent diffusion coefficient (ADC) were measured in enhanced lesions and NEPTRs. Student's t-tests and receiver operating characteristic (ROC) curves were constructed to evaluate the diagnostic performance.

RESULTS: TP lesions displayed higher Ktrans, Ve, and iAUC and lower FA and ADC values in the enhanced lesions. Moreover, significantly higher Ktrans and lower FA values were found in NEPTRs associated with TP. The Ktrans from DCE of enhanced lesions and the FA from DTI

* Guarantor and correspondent: Guihua Jiang, The Affiliated Guangdong Second Provincial General Hospital of Jinan University, School of Medicine, Jinan University, Guangzhou, 510632, China.
E-mail address: jianggh@gd2h.org.cn (G. Jiang).
† The author contributed equally to this work.

https://doi.org/10.1016/j.crad.2025.107114

of NEPTRs showed high diagnostic efficacies of 0.875 and 0.861, respectively. Notably, the area under the ROC curve of Ktrans in NEPTRs reached 0.831. The combined diagnostic performance of the three parameters reached 0.983, with 96.7% sensitivity and 92.9% specificity.

CONCLUSION: By quantifying perfusion and diffusion in enhanced lesions and NEPTRs, DCE in combination with DTI imaging can distinguish TP from TR.

Background

High-grade glioma (HGG) is the most prevalent primary malignant brain tumour in adults. Unfortunately, the prognosis for HGG remains poor, as evidenced by a five-year survival rate of less than 10%. This situation poses a significant challenge to global health.[1–4] The current treatment recommendation for HGG is primary surgical resection followed by radiotherapy or concurrent chemoradiotherapy.[1,5] Patients may develop new or enlarged contrast-enhanced lesions on routine follow-up imaging, which might be attributed to true progression (TP) or treatment response (TR).[6,7] Accurate differentiation between TP and TR is important as it can help determine whether to continue with standard adjuvant chemotherapy or to switch to a second-line therapy for recurrence.[8] Unfortunately, conventional imaging techniques cannot effectively distinguish TP from TR. Although some progress has been made through combined conventional and functional MR techniques, attention is often focused on tissues of the surgical region[9–12] and ignores non-enhanced peritumoral regions (NEPTRs). Indeed, the enhanced areas of both TP and TR are heterogeneous due to the complex microenvironment created by surgical resection. Nevertheless, NEPTRs also contain valuable information about the tumour microenvironment.[13–16] Theoretically, NEPTRs are associated with various pathological processes associated with TR and TP, including vasogenic and infiltrative oedema.[16] Using advanced MR technology to observe and explore the haemodynamic changes and indicators of tumour invasiveness in both enhanced lesions and NEPTRs is very important in differentiating TR from TP.

Angiogenesis and tumour cell infiltration are the main features of glioma and can be sensitively detected by perfusion- and diffusion-weighted magnetic resonance imaging (MRI).[17] Dynamic contrast-enhanced (DCE)-MRI provides measurements of vascular permeability, with volume transfer contrast (Ktrans), extravascular extracellular volume fraction (Ve), and Vp being the most commonly assessed parameters.[10,18–20] Very few studies have explored NEPTRs with DCE imaging. Diffusion tensor imaging (DTI) provides quantitative information such as fractional anisotropy (FA) and the apparent diffusion coefficient (ADC), which may reflect anisotropy along the white matter (WM) tracts and structured orientation and cellularity.[14,21,22] However, because the assessment of surrounding NEPTRs with DTI is highly complex, different studies have reported contradictory results.[23,24] The reason may be that the definitions of extent for NEPTRs are not uniform.[14] Therefore, in this study, we assessed NEPTRs adjacent to enhanced lesions and within a $<$3cm diameter. DCE and DTI sequences may assist in the *in vivo* assessment of neoangiogenesis and tumour infiltration. However, very few studies have focused on evaluating NEPTRs through combined DCE and DTI.

This study used DCE multiparameter quantitative characteristics of microvascular changes combined with DTI imaging to observe the FA changes of tumour spread along the white matter fibre tracts and noninvasively evaluated pathophysiological changes in enhanced lesions and NEPTRs of TP and TR. Therefore, this study aims to systematically compare the diagnostic performance of combined DCE and DTI in distinguishing TP from TR, in order to identify reliable imaging indicators that may aid accurate diagnoses and treatment decisions.

Materials and methods

Patient recruitment

From June 2022 to March 2024, we selected patients with histopathology-confirmed HGG from our radiology report database. The inclusion criteria were as follows: (1) age$>$18 years; (2) completed radiation or chemoradiation; (3) new or enlarged enhanced lesions after standard treatment; (4) available multiparametric MRI results, including DTI, DCE, and gadolinium diamine (Gd)-enhanced T1-weighted imaging (T1WI); and (5) follow-up performed in accordance with the Response Assessment in Neuro-Oncology 2.0 (RANO 2.0) criteria, which include repeated surgical resection or longitudinal clinical follow-up MRI for at least 6 months.

Exclusion criteria were as follows: (1) inadequate or poor quality MR imaging, (2) patients treated with anti-angiogenic drugs, such as bevacizumab, and (3) lost to follow-up. This retrospective study was approved by the institutional review board and eventually enrolled 44 patients.

In this study, confirmations of TR or TP were based on either histopathology from repeated surgical resection or longitudinal MRI follow-up, in accordance with the RANO 2.0 criteria for HGG.[25] Briefly, during a minimum 6-month follow-up period, TP was defined as a progressive increase

in size and/or number of enhanced lesions accompanied by deterioration of the clinical condition, and TR was defined as stable or regressing enhanced lesions and an improved clinical condition with no additional treatment. Structural and functional MRI techniques were combined to distinguish characteristic features of HGG from other primary or metastatic brain tumours, including invasive growth patterns, restricted diffusion, and elevated perfusion. Concurrently, extracranial primary malignancies were rigorously excluded through institutional standardised whole-body screening protocols incorporating positron emission tomography–computed tomography (PET-CT) and chest CT. The examination of MR images and clinical notes was performed by two neuroradiologists or neurosurgeons, and in cases of disagreement, the diagnosis was made with a third neuroradiologist who possesses over 15 years of specialised experience in neuro-oncology MRI interpretation, ensuring superior competency relative to the initial evaluators.

Image acquisition

All patients underwent examinations on a Siemens Skyra 3.0-Tesla scanner (Siemens Healthcare, Germany) with a 32-channel phased-array head coil and had an indwelling needle placed in the elbow vein. The following sequences were performed: conventional MR scan (T1WI, T2WI, and T2 fluid-attenuated inversion recovery (FLAIR)), DTI, DCE, and Gd-enhanced 3D-T1WI.

DCE-MRI was performed with a volume interpolated breath-hold examination (VIBE)-gradient echo sequence. Pre-contrast T1W VIBE sequences (repetition time (TR): 6.0 ms, echo time (TE): 2.5 ms, field of view (FOV): 340 mm×340 mm, flip angle: 5°, and slice thickness: 1.5 mm) were followed by enhanced VIBE sequences after the first five nonenhanced time phases (TR: 6.0 ms, TE: 2.5 ms, Field of View (FOV): 340 mm × 340 mm, flip angle: 10°, and slice thickness: 1.5 mm), and the gadolinium diamine was injected using a high-pressure syringe at 0.1 mmol/kg body weight and at a rate of 2-3 mL/s followed by a 40 mL saline bolus. The temporal resolution (Δt) was 4.5 s. The total acquisition time was 5 minutes, with a total of 60 periods. The DTI scans were acquired using diffusion-weighted echo-planar single-shot sequences with the following parameters: TR: 3500 ms, TE: 80 ms, FOV: 220 mm × 220 mm, 64 noncollinear gradient directions, b values = 0, 1000 s/mm^2, and slice thickness: 5 mm. The parameters of the CE 3D-T1WI scan were TR: 2300 ms, TE: 2.3 ms, FOV: 240 mm × 240 mm, and slice thickness: 1.0 mm. The post-contrast transverse T1WI were reconstructed from the transverse, coronal, and sagittal imaging.

Image analysis

The DCE images were processed on a Siemens Syngo. via workplace with Tissue 4D software (syngo. MR Tissue 4D, Siemens). We applied the Tofts and Kermode model (TK model) for the DCE-MRI data and obtained the pseudo-colour images of quantitative parameters Ktrans and Ve and semiquantitative parameter initial area under the time concentration curve (iAUC) values and fused these images with the Gd-enhanced 3D-T1WI images. As shown in supplementary Fig 1, the regions of interest (ROIs) were carefully chosen by two experienced neuroradiologists, and three to five ROIs were measured for each patient for the highest parametric values in the enhanced lesions and NEPTRs (the areas adjacent to and within 3 cm of enhanced tumour), with a size of approximately 30-50 mm^2. The ROI of enhanced lesions and NEPTRs are both taken from the brain parenchyma. Regarding DTI, Siemens Syngo.via Neuro-3D software was used to post process the original DTI data (syngo. MR Neuro 3D, Siemens). The ROIs were identified in the enhanced and peritumoral regions according to the region with the most obvious CE-T1WI. The large vessels and haemorrhagic, cystic, or large liquefactive necrotic areas were carefully avoided. The normalised FA ratio and ADC ratio were calculated by dividing the value of contralateral normal-appearing white matter.

Statistical analysis

Statistical analyses were performed with SPSS v. 26.0 (IBM Corporation). The parameters Ktrans, Ve, and iAUC of DCE-MRI and the parameters FA and ADC of DTI in the enhanced lesions and NEPTRs were compared by a Student's t-test between the groups according to the normality test. The parameters are expressed as the mean ± standard deviation. Receiver operating characteristic (ROC) curves analysed by MedCalc statistical software were used to assess the performance of statistically significant parameters. The sensitivity, specificity, and optimal cut-off values of the parameters were recorded according to Youden's index. Interobserver agreement for manually delineated ROIs was quantified via intraclass correlation coefficient (ICC) with a two-way random-effects model. $P < .05$ was considered statistically significant.

Results

This study included 44 patients. Among the 30 patients in the TP group, 19 of whom were diagnosed via histopathology, the other 11 patients were diagnosed by findings of enlarged or newly enhanced lesions and deteriorating clinical symptoms during a follow-up period of more than 6 months. Among the 14 patients in the TR group, 12 had stable or improved clinical symptoms and stable or regressed lesions on MRI after more than 6 months of follow-up, 2 patients with TR were diagnosed via histopathology.

The ICC values of all of the parameters were greater than 0.75, indicating a good correlation. The Ktrans, Ve, iAUC, ADC, and FA values calculated for the enhanced lesions and NEPTRs of HGG patients with TP or TR are summarised in Table 1. In the enhanced lesions, the Ktrans, Ve, and iAUC were significantly higher in the TP than in the TR (< .05). Both the FA and ADC were significantly lower in TP than in TR (< .05). Additionally, we observed that the Ktrans values were significantly higher and the FA values were

Table 1
Comparison of parameters in the enhanced lesions and NEPTRs of the TP and TR groups.

	TP (n=30)	TR (n=14)	*p*
Enhanced lesions			
Ktrans (min^{-1})	0.217 ± 0.060	0.102 ± 0.073	**<0.001**
Ve	0.514 ± 0.242	0.266 ± 0.117	**<0.001**
iAUC (mmol/L.min)	0.110 ± 0.047	0.066 ± 0.031	**0.003**
rFA	0.443 ± 0.185	0.624 ± 0.274	**0.036**
rADC ($\times 10^{-3}$ mm^2/s)	0.847 ± 0.299	1.084 ± 0.330	**0.022**
NEPTRs			
Ktrans	0.117 ± 0.119	0.049 ± 0.025	**0.042**
Ve	0.202 ± 0.139	0.157 ± 0.120	0.308
iAUC	0.052 ± 0.046	0.050 ± 0.023	0.877
rFA	0.470 ± 0.201	0.829 ± 0.251	**<0.001**
rADC	1.265 ± 0.253	1.370 ± 0.252	0.204

ADC, apparent diffusion coefficient; **iAUC,** initial area under the time concentration curve; **FA,** fractional anisotropy; **Ktrans,** volume transfer contrast; **NEPTRs,** non-enhancing peritumoral regions; **TP,** true progression; **TR,** treatment response; **Ve,** extravascular extracellular volume fraction. *P* values < 0.05 are labelled in bold.

significantly lower in the NEPTRs of TP lesions than in the NEPTRs of TR lesions. Furthermore, no statistical differences were identified for Ve, iAUC, or ADC in NEPTRs of TP and TR (*P*>.05). Supplementary Figs 2 and 3 illustrate representative cases from each group. The difference between TR and TP groups for each parameter is shown in Fig 1.

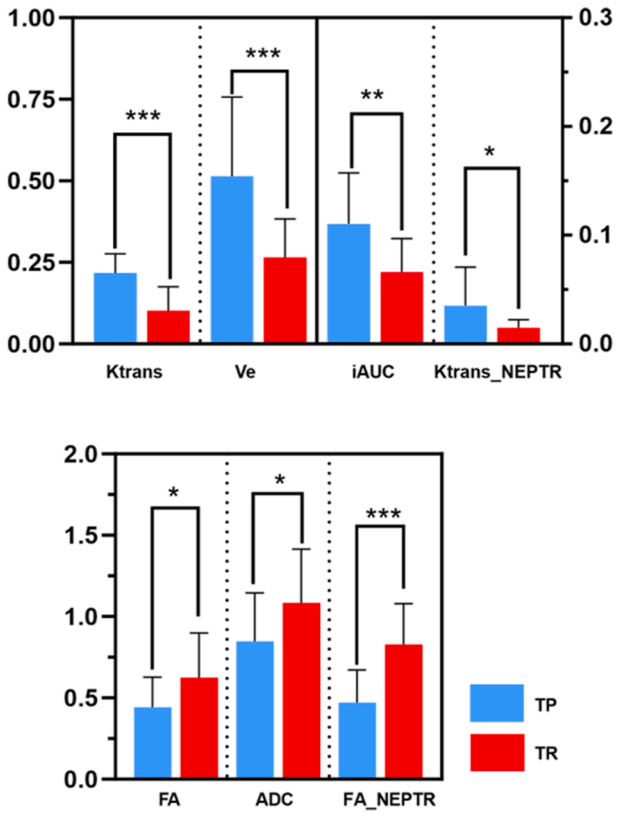

Figure 1 Comparison of magnetic resonance imaging (MRI) parameters for the tumour progression (TP) and treatment response (TR) groups. *** < .001, ** < .01, * < .05.

Table 2
The diagnostic performance of multiparameter imaging in distinguishing TP from TR.

	Cut-off value	Sensitivity (%)	Specificity (%)	AUC
Ktrans (min^{-1})	0.15	90.0	78.6	0.875
Ve	0.38	73.3	85.7	0.811
iAUC(mmol/L.min)	0.05	93.3	50.0	0.771
rFA	0.63	90.0	57.1	0.704
rADC	0.89	63.3	78.6	0.707
$Ktrans_{NEPTR}$	0.07	80.0	78.6	0.831
rFA_{NEPTR}	0.73	90.0	71.4	0.861
Ktrans + $Ktrans_{NEPTR}$ + FA_{NEPTR}	-	96.7	92.9	0.983

ADC, apparent diffusion coefficient; **FA,** fractional anisotropy; **iAUC,** initial area under the time concentration curve; **Ktrans,** volume transfer contrast; **NEPTRs,** non-enhancing peritumoral regions; **Ve,** extravascular extracellular volume fraction.

The results of the ROC curve analyses for the above parameters are presented in Table 2 and Fig 2. A logistic regression analysis was employed to evaluate the combined performance of Ktrans and FA, which had the highest diagnostic efficiency in differentiating TP from TR. As shown in Table 2 and Fig 2, Ktrans in the enhanced lesions and NEPTRs demonstrated high diagnostic performance and an optimal balance between sensitivity and specificity with cut-off values of 0.15/min and 0.07/min, respectively. FA in the NEPTRs demonstrated high diagnostic performance and an optimal balance between sensitivity and specificity with a threshold of 0.73. Moreover, the combination of Ktrans + Ktrans_NEPTRs + FA_NEPTRs yielded the highest area under the ROC curve (AUC, 0.983), which were higher than those of any single parameter (Fig 3).

Discussion

Distinguishing TR from TP presents challenges but remains crucial for guiding treatment decisions as differentiation can help determine whether to continue with standard adjuvant chemotherapy or to switch to a second-line therapy for recurrence.[9,26] In the present study, we used DCE and DTI sequences to quantify the changes in vascular permeability and water molecular diffusion, which assists in diagnosis of TR and TP by identifying the different mechanisms underlying the pathological changes. Our results demonstrated that the enhanced lesions of TP presented higher Ktrans, Ve, and iAUC values and lower FA and ADC values than the enhanced lesions of TR. In addition, the NEPTRs of TP lesions also presented higher Ktrans values and lower FA values. Furthermore, these parameters were effective in distinguishing between TP and TR in HGG patients who had received only conventional chemoradiotherapy.

In the present study, we found that Ktrans, Ve, and iAUC all had high diagnostic efficacy for enhanced lesions, which is consistent with the findings of previous studies.[18,27] The results indicated that there was substantial

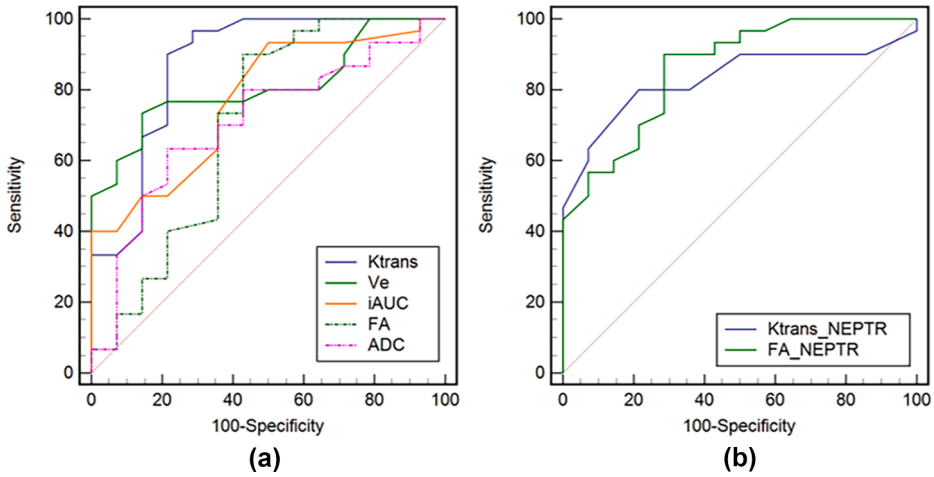

Figure 2 ROC curves of Ktrans, Ve, iAUC, FA, and ADC values in the enhanced lesions (a) and NEPTRs (b) as used for differentiating TP from TR. **ADC,** apparent diffusion coefficient; **FA,** fractional anisotropy; **iAUC,** initial area under the time concentration curve; **Ktrans,** volume transfer contrast; **NEPTRs,** non-enhancing peritumoral regions; ROC, receiver operating characteristic.

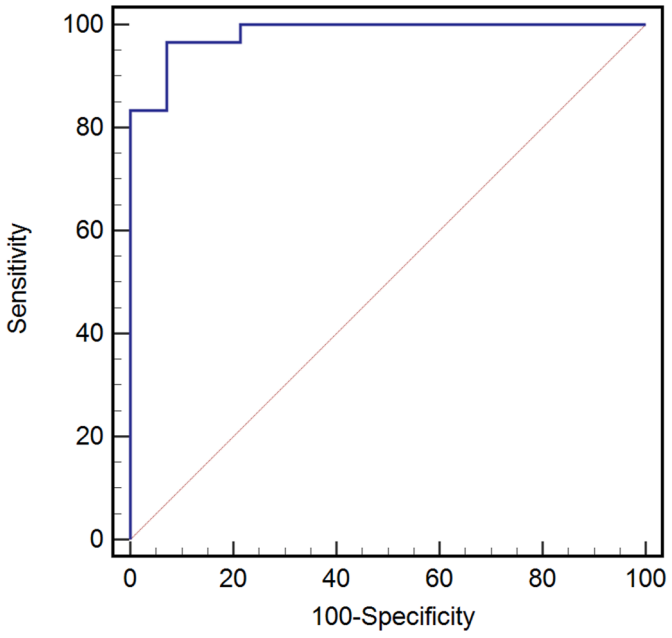

Figure 3 ROC curves of the combined parameters (Ktrans + $Ktrans_{NEPTR}$ + FA_{NEPTR}) used for differentiating TP from TR. **FA,** fractional anisotropy; **iAUC,** initial area under the time concentration curve; **Ktrans,** volume transfer contrast; **NEPTRs,** non-enhancing peritumoral regions; ROC, receiver operating characteristic.

neovascularization in the parenchymal area of TPs. On the other hand, TR is thought to be a marker of tumour sensitivity to radiation and chemotherapy and is associated with low-angiogenic regions and vasogenic oedema due to disruption of the blood–brain barrier.[28] Notably, despite high diagnostic efficacy, the trend of Ve values has been inconsistent among the studies.[29–31] Our findings demonstrate a significant increase in Ve values among patients with TP, which is consistent with the findings of Yun *et al.*[30] This likely reflects abnormal and chaotic architecture of a tumour tissue, which is often characterized by necrotic areas. However, some studies have shown an opposite trend and were explained that Ve is inversely proportional to angiogenesis and high cellularity. In parallel, our findings demonstrated that the Ktrans of NEPTRs exhibited excellent diagnostic performance, which has not been reported in previous studies.[32] This may indicate increased vessel density, abnormally structured tumoural blood vessels, and an impaired blood–brain barrier as a consequence of neoangiogenesis in NEPTRs.[33,34] Additionally, although there was no significant difference in Ve and iAUC in NEPTRs, a slight tendency towards higher values in TP-associated NEPTRs was observed. This finding supports a mechanism of microvascularization in the infiltration zone during tumour recurrence. Thus, DCE-MRI can provide useful perfusion information about both enhanced lesions and NEPTRs and can allow differentiation between TP and TR, thereby aiding appropriate clinical management.

In our study, the FA values in enhanced lesions diagnosed as TP were lower than those in TR but the diagnostic performance of FA values was slightly inferior to that of DCE parameters, which is consistent with the results of previous studies. Nevertheless, several studies have reported null or opposite tendencies in anisotropy measures of TP and TR.[21,35] This discrepancy may be due to disrupted postoperative architectures of solid components. Interestingly, our results also revealed a notable difference in the FA of NEPTRs in the two groups that had excellent diagnostic efficiency compared with the FA of enhanced lesions. This result suggested a distinguishable difference between tumour infiltration and vasogenic oedema, where lower FA values in NEPTRs associated with recurrence were due to the tumoural destruction of white fibres. Only a few previous studies have investigated NEPTRs after glioma

surgery, and our results differ from the results of Razek *et al.*[35] due to our different definition of the extent of NEPTRs. Our choice to consider a 3 cm diameter was motivated by the fact that invasive glioma cells can reach 3 cm beyond the enhanced tumour in MRI sequences,[36] and our distance also covers high-frequency recurrence regions.[37] The ADC value derived from DTI was also used to quantify cellularity. Our study found that there was a difference in the enhanced lesions but the diagnostic performance was limited. Generally, tumour cell proliferation leads to a reduction in diffusivity, and restricted water diffusion is reflected by decreased ADC values. Our results could be explained as follows: increased cellularity in the lesions of patients with TP inhibits water molecule diffusion, thereby restricting diffusion. Additionally, TR lesions are characterized by high viscosity and inflammatory cellular composition, such as polymorphonuclear leukocytes, which limits the diffusion of water. However, differences in the ADC of the TP and TR NEPTRs was not significant and could not distinguish TP from TR, which is consistent with the previous study.[38]

Moreover, given that both the Ktrans value and FA value had good diagnostic efficacy and reflected different tumour histopathological factors, including vascular proliferation and cell dissemination, the Ktrans value could complement the FA value in distinguishing TP from TR. By combining the Ktrans of enhanced lesions and NEPTRs with the FA of NEPTRs, the sensitivity, specificity, and diagnostic performance was substantially improved, with an AUC of 0.983 (95% CI: 0.890-1.000). The higher sensitivity and specificity values indicate that Ktrans and FA values can serve as reliable markers for distinguishing TP from TR.

This study has several limitations. First, there were a limited number of subjects, especially in the TR group. However, the enrolled subjects were nearly homogeneous, and the results obtained were significant and encouraging. Second, there were fewer histopathological results because of the aforementioned tissue components and changes after radiation therapy, which made puncture biopsies of TR lesions less accurate. In addition, this study included both pseudoprogression and radionecrosis as TR without precisely dividing them. Despite having distinct clinical and pathophysiological mechanisms, they share many histological similarities, such as inflammatory infiltrates and necrosis, which translate into similar imaging characteristics.

Conclusions

In summary, our study investigated the use of DCE and DTI as noninvasive tools for distinguishing between TP and TR in HGG patients. Evaluation of NEPTRs can provide significant information for HGG patients who have received only conventional chemoradiotherapy. The increased sensitivity and specificity of combined parameters suggests their potential as reliable indicators. Combining DCE and DTI can improve the accuracy of diagnosis and aid patients with new or advancing enhanced lesions in formulating accurate treatment plans with their physicians.

Author contributions

The contribution of each author is presented as follows:

1. **Yanzhao Diao, Guihua Jiang, Hexin Liang, Yuqi Wang, Lifeng Hang, Laiping Fang, Hong Qu, Hui Sun, and Wenjing Li** contributed as guarantor of integrity of the entire study.
2. **Yanzhao Diao, Guihua Jiang, and Hexin Liang** contributed to Study concepts and design .
3. **Hesxin Liang, Yuqi Wang, and Guihua Jiang** contributed to literature research.
4. **Lifeng Hang and Laiping Fang** contributed to clinical studies.
5. **Yanzhao Diao, Hong Qu, Hui Sun, andWenjing Li** contributed to experimental studies/data analysis.
6. **Yanzhao Diao, Hexin Liang** contributed to statistical analysis.
7. **Yanzhao Diao, Hexin Liang** contributed to the manuscript.
8. **Guihua Jiang** contributed to manuscript editing.

Ethical statement

The study was conducted in accordance with the Declaration of Helsinki (as revised in 2013). All patients signed an informed consent form for the DCE and DTI examination. The data applied in this study were exempted from ethical review due to the retrospective nature.

Conflict of interests

The authors declare that they have no known competing financial interests or personal relationships that could have appeared to influence the work reported in this paper.

Acknowledgments

This work was supported by the National Natural Science Foundation of China (82271948; 82371913), Funding by Science and Technology Projects in Guangzhou (2025A04J4629), Fujian Province Science and Technology Plan (2024D022), and 2024 Smart Imaging New Technology Innovation Fund (NMED2024CX-01-005).

Appendix A. Supplementary data

Supplementary data to this article can be found online at https://doi.org/10.1016/j.crad.2025.107114.

Abbreviations

HGG
: high-grade glioma

TP
: true progression

TR
: treatment response

NEPTRs
non-enhancing peritumoral regions
DCE-MRI
dynamic contrast-enhanced magnetic resonance imaging
DTI
diffusion tensor imaging
ROC
receiver operating characteristic
AUC
area under the ROC curve
Ktrans
volume transfer contrast
Ve
extravascular extracellular volume fraction
iAUC
initial area under the time concentration curve
FA
fractional anisotropy
ADC
apparent diffusion coefficient
ROI
region of interest
CNAWM
contralateral normal-appearing white matter
Gd
gadolinium
RANO
Response Assessment in Neuro-Oncology
SD
standard deviation

References

1. Angom RS, Nakka NMR, Bhattacharya S. Advances in glioblastoma therapy: an update on current approaches. *Brain Sci* 2023;**13**:1536.
2. Huang-Hobbs E, Cheng Y-T, Ko Y, *et al*. Remote neuronal activity drives glioma progression through SEMA4F. *Nature* 2023;**619**:844–50.
3. Omuro A, DeAngelis LM. Glioblastoma and other malignant gliomas: a clinical review. *Jama* 2013;**310**:1842–50.
4. Qu H, Zeng Y, Hang L, *et al*. Simultaneously acquired rSUV and rCBF of 18F-FDG/MRI in peritumoral brain zone can help to differentiate the grade of gliomas. *Meta-Radiol* 2023;**1**.
5. Fernandes C, Costa A, Osório L, *et al*. *Current standards of care in glioblastoma therapy*. Exon Publications; 2017. p. 197–241.
6. Henriksen OM, del Mar Álvarez-Torres M, Figueiredo P, *et al*. High-grade glioma treatment response monitoring biomarkers: a position statement on the evidence supporting the use of advanced MRI techniques in the clinic, and the latest bench-to-bedside developments. Part 1: perfusion and diffusion techniques. *Frontiers in Oncol* 2022;**12**:810263.
7. Hu LS, Smits M, Kaufmann TJ, *et al*. Advanced imaging in the diagnosis and response assessment of high-grade glioma: AJR Expert Panel narrative review. *AJR Am J Roentgenol* 2025;**224**(1):e2330612.
8. Rogozińska E, Kernohan A, Robinson T, *et al*. Treatment options for progression or recurrence of glioblastoma: a network meta-analysis. *Cochrane Database Syst Rev* 2021.
9. van Dijken BR, van Laar PJ, Holtman GA, *et al*. Diagnostic accuracy of magnetic resonance imaging techniques for treatment response evaluation in patients with high-grade glioma, a systematic review and meta-analysis. *European Radiology* 2017;**27**:4129–44.
10. Bisdas S, Naegele T, Ritz R, *et al*. Distinguishing recurrent high-grade gliomas from radiation injury: a pilot study using dynamic contrast-enhanced MR imaging. *Acad Radiol* 2011;**18**:575–83.
11. Stockham AL, Tievsky AL, Koyfman SA, *et al*. Conventional MRI does not reliably distinguish radiation necrosis from tumor recurrence after stereotactic radiosurgery. *J Neuro-Oncol* 2012;**109**:149–58.
12. Moltoni G, Romano A, Capriotti G, *et al*. ASL, DSC, DCE perfusion MRI and 18F-DOPA PET/CT in differentiating glioma recurrence from post-treatment changes. *La Radiologia Medica* 2024:1–12.
13. Durst CR, Raghavan P, Shaffrey ME, *et al*. Multimodal MR imaging model to predict tumor infiltration in patients with gliomas. *Neuroradiology* 2014;**56**:107–15.
14. Bette S, Huber T, Gempt J, *et al*. Local fractional anisotropy is reduced in areas with tumor recurrence in glioblastoma. *Radiology* 2017;**283**:499–507.
15. Xing Z, Wang C, Yang W, *et al*. Predicting glioblastoma recurrence using multiparametric MR imaging of non-enhancing peritumoral regions at baseline. *Heliyon* 2024;**10**:e30411.
16. Artzi M, Bokstein F, Blumenthal DT, *et al*. Differentiation between vasogenic-edema versus tumor-infiltrative area in patients with glioblastoma during bevacizumab therapy: a longitudinal MRI study. *Eur J Radiol* 2014;**83**:1250–6.
17. Autry A, Phillips JJ, Maleschlijski S, *et al*. Characterization of metabolic, diffusion, and perfusion properties in GBM: contrast-enhancing versus non-enhancing tumor. *Translational Oncol* 2017;**10**:895–903.
18. Thomas AA, Arevalo-Perez J, Kaley T, *et al*. Dynamic contrast enhanced T1 MRI perfusion differentiates pseudoprogression from recurrent glioblastoma. *J Neuro-Oncol* 2015;**125**:183–90.
19. Qiu J, Tao Z-C, Deng K-X, *et al*. Diagnostic accuracy of dynamic contrast-enhanced magnetic resonance imaging for distinguishing pseudoprogression from glioma recurrence: a meta-analysis. *Chinese Med J* 2021;**134**:2535–43.
20. Okuchi S, Rojas-Garcia A, Ulyte A, *et al*. Diagnostic accuracy of dynamic contrast-enhanced perfusion MRI in stratifying gliomas: a systematic review and meta-analysis. *Cancer Med* 2019;**8**:5564–73.
21. Wang S, Martinez-Lage M, Sakai Y, *et al*. Differentiating tumor progression from pseudoprogression in patients with glioblastomas using diffusion tensor imaging and dynamic susceptibility contrast MRI. *Am Jf Neuroradiol* 2016;**37**:28–36.
22. Metz M-C, Molina-Romero M, Lipkova J, *et al*. Predicting glioblastoma recurrence from preoperative MR scans using fractional-anisotropy maps with free-water suppression. *Cancers* 2020;**12**:728.
23. Stadlbauer A, Ganslandt O, Buslei R, *et al*. Gliomas: histopathologic evaluation of changes in directionality and magnitude of water diffusion at diffusion-tensor MR imaging. *Radiology* 2006;**240**:803–10.
24. Hoefnagels FW, De Witt Hamer P, Sanz-Arigita E, *et al*. Differentiation of edema and glioma infiltration: proposal of a DTI-based probability map. *J Neuro-Oncol* 2014;**120**:187–98.
25. Wen PY, van den Bent M, Youssef G, *et al*. Rano 2.0: update to the response assessment in neuro-oncology criteria for high-and low-grade gliomas in adults. *J Clin Oncol* 2023;**41**:5187–99.
26. Feng A, Yuan P, Huang T, *et al*. Distinguishing tumor recurrence from radiation necrosis in treated glioblastoma using multiparametric MRI. *Acad Radiol* 2022;**29**:1320–31.
27. Seeger A, Braun C, Skardelly M, *et al*. Comparison of three different MR perfusion techniques and MR spectroscopy for multiparametric assessment in distinguishing recurrent high-grade gliomas from stable disease. *Acad Radiol* 2013;**20**:1557–65.
28. Zikou A, Sioka C, Alexiou GA, *et al*. Radiation necrosis, pseudoprogression, pseudoresponse, and tumor recurrence: imaging challenges for the evaluation of treated gliomas. *Contrast Media Mol Imag* 2018;**2018**:6828396.
29. Lüdemann L, Grieger W, Wurm R, *et al*. Quantitative measurement of leakage volume and permeability in gliomas, meningiomas and brain metastases with dynamic contrast-enhanced MRI. *Mag Reson Imag* 2005;**23**:833–41.
30. Yun TJ, Park C-K, Kim TM, *et al*. Glioblastoma treated with concurrent radiation therapy and temozolomide chemotherapy: differentiation of true progression from pseudoprogression with quantitative dynamic contrast-enhanced MR imaging. *Radiology* 2015;**274**:830–40.
31. Jing H, Yan X, Li J, *et al*. The value of dynamic contrast-enhanced magnetic resonance imaging (DCE-MRI) in the differentiation of pseudoprogression and recurrence of intracranial gliomas. *Contrast Media Mol Imag* 2022;**2022**:5680522.
32. Lundemann M, Munck af Rosenschöld P, Muhic A, *et al*. Feasibility of multi-parametric PET and MRI for prediction of tumour recurrence in patients with glioblastoma. *Eur J Nuclear Med Mol Imag* 2019;**46**:603–13.

33. Jain R, Griffith B, Alotaibi F, *et al*. Glioma angiogenesis and perfusion imaging: understanding the relationship between tumor blood volume and leakiness with increasing glioma grade. *Am J Neuroradiol* 2015;**36**:2030–5.
34. Heo D, Lee J, Yoo R-E, *et al*. Deep learning based on dynamic susceptibility contrast MR imaging for prediction of local progression in adult-type diffuse glioma (grade 4). *Sci Rep* 2023;**13**:13864.
35. Razek AAKA, El-Serougy L, Abdelsalam M, *et al*. Differentiation of residual/recurrent gliomas from postradiation necrosis with arterial spin labeling and diffusion tensor magnetic resonance imaging-derived metrics. *Neuroradiol* 2018;**60**:169–77.
36. Kolakshyapati M, Adhikari RB, Karlowee V, *et al*. Nonenhancing peritumoral hyperintense lesion on diffusion-weighted imaging in glioblastoma: a novel diagnostic and specific prognostic indicator. *J Neurosurg* 2017;**128**:667–78.
37. Liu D, Chen J, Ge H, *et al*. Differentiation of malignant brain tumor types using intratumoral and peritumoral radiomic features. *Front Oncol* 2022;**12**:848846.
38. Sundgren PC, Fan X, Weybright P, *et al*. Differentiation of recurrent brain tumor versus radiation injury using diffusion tensor imaging in patients with new contrast-enhancing lesions. *Mag Reson Imag* 2006;**24**:1131–42.